

On Robust Classification using Contractive Hamiltonian Neural ODEs

Muhammad Zakwan, Liang Xu and Giancarlo Ferrari-Trecate

Abstract—Deep neural networks can be fragile and sensitive to small input perturbations that might cause a significant change in the output. In this paper, we employ contraction theory to improve the robustness of neural ODEs (NODEs). A dynamical system is contractive if all solutions with different initial conditions converge to each other asymptotically. As a consequence, perturbations in initial conditions become less and less relevant over time. Since in NODEs, the input data corresponds to the initial condition of dynamical systems, we show contractivity can mitigate the effect of input perturbations. More precisely, inspired by NODEs with Hamiltonian dynamics, we propose a class of contractive Hamiltonian NODEs (CH-NODEs). By properly tuning a scalar parameter, CH-NODEs ensure contractivity by design and can be trained using standard backpropagation and gradient descent algorithms. Moreover, CH-NODEs enjoy built-in guarantees of non-exploding gradients, which ensures a well-posed training process. Finally, we demonstrate the robustness of CH-NODEs on the MNIST image classification problem with noisy test datasets.

I. INTRODUCTION

Neural networks (NNs) have demonstrated stunning performance in image classification, natural language processing, and speech recognition tasks. However, they can be sensitive to input noise or adversarial attacks [1]. For example, in image classification problems using Convolutional Neural Networks (CNNs), it has been shown that adding a small perturbation to an input image can lead to misclassification [2]. The common solutions are either heuristic, for example, feature obfuscation [3] and adversarial training [4], or certificate-based such as Lipschitz regularization [1], [5] penalizing the Lipschitz constant of each NN layer. Likewise, the notion of incremental dissipativity is employed to generalize Lipschitz-based robustness certificates for NNs [6]. The general purpose of certificate-based techniques is to penalize the input-to-output sensitivity of a NN to improve robustness. To do so, they usually require layerwise regularization, which is computationally expensive.

Recently, the connection between NNs and dynamical systems has been extensively explored. Representative results include classes of NNs stemming from the discretization of dynamical systems [7] and Neural ODEs (NODEs) [8]. Instead of specifying a discrete sequence of hidden layers, NODEs transform the input through a continuous-time ODE embedding training parameters. The continuous-time nature of NODEs makes them particularly suitable for learning the

complex dynamical systems [9], [10] and allows borrowing tools from the system theory to analyze NN properties.

Although NODEs have shown greater robustness against random perturbations than common CNNs [11], research on methods guaranteeing more robustness is still very active. Several works adopted system theoretic perspective and proposed robustness promoting techniques for NODEs. For instance, to improve resilience to adversarial attacks, NODEs equipped with Lyapunov-stable equilibrium points have been proposed [12]. Likewise, [13] introduces a loss function to promote robustness based on a control-theoretic Lyapunov condition. Both methods have shown promising performance against adversarial attacks. Nonetheless, they do not exhibit robustness guarantees *by design*.

In this paper, we employ contraction theory to enhance the robustness of NODEs. A dynamical system is contractive if all trajectories converge to each other asymptotically [14], [15]. From the lens of contraction, slight perturbations of initial conditions have a diminishing impact over time on the NODE state. We highlight that the notion of contractivity allows one to deal with non-autonomous systems while studying the stability of multiple trajectories at once. Contractivity has been used to improve the well-posedness of implicit neural networks [16] and the trainability of recurrent neural networks [17]. Nevertheless, to the authors' knowledge, the relation between contractivity and robustness of NODEs has not been exploited.

With the above considerations, we propose a class of NODEs with built-in contraction properties based on the theory of Hamiltonian systems, which we refer to as contractive Hamiltonian NODEs (CH-NODEs). Hamiltonian systems are structured nonlinear systems that can model complex dynamics [18]. Since their built-in dissipation properties facilitate contraction analysis, they are natural candidates for building contractive NODEs. Moreover, CH-NODEs do not rely on stability-promoting regularizers/costs [12], [13], which can increase the training complexity, hence limiting the depth of the NNs that can be used in applications. In general, NODEs rely on gradient based algorithms to update weights. The appearance of vanishing or exploding gradient during training may cause numerical instability, thus compromising the learning process. We however prove that CH-NODEs cannot have exploding gradients, irrespective of their depth and for all possible values of the parameters. Finally, we test CH-NODEs in benchmark classification problems and show that they can achieve substantially better accuracy than alternative architectures on test dataset corrupted by noises.

Notation. The operator $\frac{\partial^2 f(\mathbf{x})}{\partial \mathbf{x}^2}$ denotes the Hessian of a continuously differentiable function $f(\cdot)$. The maximal and

This research is supported by the Swiss National Science Foundation under the NCCR Automation (grant agreement 51NF40 180545).

Authors are with the Institute of Mechanical Engineering, Ecole Polytechnique Fédérale de Lausanne (EPFL), CH-1015 Lausanne, Switzerland {muhammad.zakwan, liang.xu, giancarlo.ferrari-trecate}@epfl.ch

minimal eigenvalues of a matrix \mathbf{A} are denoted as $\bar{\lambda}(\mathbf{A})$ and $\underline{\lambda}(\mathbf{A})$, respectively. $\text{diag}(\mathbf{x})$ represents a diagonal matrix with the entries of the vector \mathbf{x} on the diagonal. The set of non-negative real numbers is \mathbb{R}^+ .

Organization: This paper is organized as follows: Section 2 provides the preliminaries. In Section 3, we introduce and analyze CH-NODEs. The performance evaluation is conducted in Section 4 and Section 5 concludes the paper.

II. PRELIMINARIES

We briefly introduce NODEs and describe how contractivity can improve their robustness. Moreover, we recall a few preliminaries related to Hamiltonian systems.

A. Neural ODEs

A neural ODE [8] is a continuous-depth model defined by

$$\boldsymbol{\xi}(0) = \phi(\mathbf{x}, \omega), \quad (\text{input layer}) \quad (1)$$

$$\dot{\boldsymbol{\xi}}(t) = f_t(\boldsymbol{\xi}(t), \theta(t)), \quad (\text{continuum of hidden layers}) \quad (2)$$

$$\mathbf{y}(T) = \psi(\boldsymbol{\xi}(T), \eta), \quad (\text{output layer}) \quad (3)$$

where $\mathbf{x} \in \mathbb{R}^m$ is the input data (e.g an image), $\boldsymbol{\xi} \in \mathbb{R}^n$ represents the state of the NODE, and ϕ, f, ψ are neural networks with trainable parameters ω, θ, η . The dynamics (2) evolves over the time interval $[0, T]$ and $\mathbf{y}(T)$ is the output. The training of NODEs (1)-(3) refers to minimizing a given loss function over trainable parameters.

Remark 1: To specify a NN architecture for the training, one can discretize the ODE (2) with a sampling period $h = \frac{T}{N}$, $N \in \mathbb{N}$. The N resulting discrete-time equations can be utilized to define the layers of a NN of depth N [8]. For instance, using Forward Euler (FE) discretization with a step-size of h , one obtains

$$\boldsymbol{\xi}_{i+1} = \boldsymbol{\xi}_i + hf_i(\boldsymbol{\xi}_i, \theta_i), \quad \text{for } i = 0, 1, \dots, N-1, \quad (4)$$

where $\boldsymbol{\xi}_i$ and $\boldsymbol{\xi}_{i+1}$ represent the input and output of layer i , respectively. In practice, one chooses the step-size h sufficiently small, so as to interpret the states in (4) as a sampled version of the state $\boldsymbol{\xi}(t)$ in (2).

Neural ODEs are not necessarily robust, as input perturbations can produce a significant change in outputs [11]. In the following, we introduce contraction theory for dynamical systems and show how it can be used for improving the robustness of NODEs.

B. Contraction theory

The definition of contraction for (2) is stated below.

Definition 1 ([14]): Let $\boldsymbol{\xi}(t)$ and $\tilde{\boldsymbol{\xi}}(t)$ be two solutions of (2) starting from $\boldsymbol{\xi}(0)$ and $\tilde{\boldsymbol{\xi}}(0)$, respectively. Then (2) is contractive if $\exists C, \rho > 0$, such that

$$\|\tilde{\boldsymbol{\xi}}(t) - \boldsymbol{\xi}(t)\| \leq Ce^{-\rho t} \|\tilde{\boldsymbol{\xi}}(0) - \boldsymbol{\xi}(0)\| \quad (5)$$

for all $t > 0$.

According to Definition (1), if the ODE (2) is contractive, then perturbations in initial conditions vanish exponentially fast. This guarantees that small perturbations in the input data $\boldsymbol{\xi}(0)$ are filtered out more and more effectively as t increases.

Remark 2: All the solution trajectories of a contractive NODE converge asymptotically to an equilibrium trajectory, which may compromise the performance of the learning task. However, this might be unavoidable for building robust neural networks, since there exists an inherent trade-off between robustness and accuracy [19]. Moreover, one can carefully select the time horizon T and the contraction rate ρ to balance the robustness and accuracy requirements. We will illustrate this trade-off through experiments in Section IV.

C. Hamiltonian System Theory

A Hamiltonian system [20] is described by

$$\dot{\boldsymbol{\xi}}(t) = (\mathbf{J}(\boldsymbol{\xi}(t)) - \mathbf{R}(\boldsymbol{\xi}(t))) \frac{\partial H(\boldsymbol{\xi}(t), t)}{\partial \boldsymbol{\xi}(t)}, \quad (6)$$

where $\mathbf{J}(\boldsymbol{\xi}(t)) = -\mathbf{J}^\top(\boldsymbol{\xi}(t))$, and $\mathbf{R}(\boldsymbol{\xi}(t)) = \mathbf{R}^\top(\boldsymbol{\xi}(t)) \geq 0$ are interconnection and damping matrices, respectively. The continuously differentiable function $H : \mathbb{R}^n \times \mathbb{R}^+ \rightarrow \mathbb{R}$ is called the *Hamiltonian*, and can be interpreted as the energy of the system (6). It is straightforward to show that,

$$\dot{H}(t) = -\frac{\partial H^\top(\boldsymbol{\xi}(t), t)}{\partial \boldsymbol{\xi}(t)} \mathbf{R}(\boldsymbol{\xi}(t)) \frac{\partial H(\boldsymbol{\xi}(t), t)}{\partial \boldsymbol{\xi}(t)} \leq 0.$$

Therefore, the system (6) is dissipating energy and $\mathbf{R}(\boldsymbol{\xi}(t))$ determines the dissipation rate. In the next section, we will illustrate how to exploit these properties to guarantee contractivity.

III. CONTRACTIVE HAMILTONIAN NEURAL ODES

In this section, we introduce CH-NODEs and show that their parameterization allows one to perform training using standard gradient based algorithms. Moreover, we show that CH-NODEs enjoy built-in guarantees of non-exploding gradients.

Consider the following NODE ¹

$$\begin{aligned} \dot{\boldsymbol{\xi}}(t) = & \mathbf{F}(t, \boldsymbol{\xi}(t)) \left(\mathbf{K}^\top(t) \tanh(\mathbf{K}(t)\boldsymbol{\xi}(t) + \mathbf{b}(t)) \right. \\ & \left. + (\mathbf{L}(t)^\top \mathbf{L}(t) + \kappa \mathbf{I}) \boldsymbol{\xi}(t) \right), \quad t \in [0, T], \end{aligned} \quad (7)$$

where \mathbf{F} is a given matrix-valued function, $\kappa > 0$ is a constant, $\mathbf{K} : \mathbb{R}^+ \rightarrow \mathbb{R}^{n \times n}$, $\mathbf{b} : \mathbb{R}^+ \rightarrow \mathbb{R}^n$, and $\mathbf{L} : \mathbb{R}^+ \rightarrow \mathbb{R}^{n \times n}$ are trainable parameters. One can easily verify that (7) is a Hamiltonian system when $\mathbf{F}(t, \boldsymbol{\xi}(t)) = \mathbf{J}(\boldsymbol{\xi}(t)) - \mathbf{R}(\boldsymbol{\xi}(t))$ for some anti-symmetric matrix $\mathbf{J}(\boldsymbol{\xi}(t))$ and positive semi-definite matrix $\mathbf{R}(\boldsymbol{\xi}(t))$. Indeed, in such case, by choosing the Hamiltonian in (6) as

$$\begin{aligned} H(\boldsymbol{\xi}(t), t) = & \log(\cosh(\mathbf{K}(t)\boldsymbol{\xi}(t) + \mathbf{b}(t)))^\top \mathbf{1}_n \\ & + \boldsymbol{\xi}^\top(t) (\mathbf{L}^\top(t) \mathbf{L}(t) + \kappa \mathbf{I}) \boldsymbol{\xi}(t), \quad t \in [0, T], \end{aligned} \quad (8)$$

where $\mathbf{1}_n$ represents a column vector with n elements equal to 1, one obtains the ODE (7).

¹We omit input and output layers for brevity. They are usually selected depending on the specific learning task.

A. Contractive Hamiltonian Neural ODEs

We show that for a suitable selection of parameters in (7), one obtains a contractive NODE by design. This result is provided by the following theorem, whose proof is given in Appendix VI-A.

Theorem 1: For a given constant skew-symmetric matrix \mathbf{J} , let \mathbf{F} in (7) be equal to $\mathbf{J} - \gamma\mathbf{I}$ and define

$$c_1 = \inf_{s \in [0, T]} \underline{\lambda}(\mathbf{L}^\top(s)\mathbf{L}(s)) + \kappa, \quad (9)$$

$$c_2 = \sup_{s \in [0, T]} (\bar{\lambda}(\mathbf{L}^\top(s)\mathbf{L}(s)) + \bar{\lambda}(\mathbf{K}^\top(s)\mathbf{K}(s))) + \kappa, \quad (10)$$

$$\alpha = \frac{c_2 - c_1}{c_2 + c_1}.$$

If $\epsilon > 0$ is such that $1 - \alpha^2 - \epsilon > 0$ and γ verifies

$$\gamma \geq \sqrt{\frac{(\alpha^2 + \epsilon)\bar{\lambda}(\mathbf{J}\mathbf{J}^\top)}{1 - \alpha^2 - \epsilon}}, \quad (11)$$

then, the NODE (7) becomes

$$\begin{aligned} \dot{\boldsymbol{\xi}}(t) = (\mathbf{J} - \gamma\mathbf{I}) & \left(\mathbf{K}^\top(t) \tanh(\mathbf{K}(t)\boldsymbol{\xi}(t) + \mathbf{b}(t)) \right. \\ & \left. + (\mathbf{L}(t)^\top\mathbf{L}(t) + \kappa\mathbf{I})\boldsymbol{\xi}(t) \right), \quad t \in [0, T], \end{aligned} \quad (12)$$

and is contractive.

The essence of Theorem 1 lies in scaling the dissipation term γ as in (11), such that the NODE (12) remains contractive for arbitrary weights. However, the selection of γ relies on NODE parameters $\mathbf{K}(t), \mathbf{L}(t)$, which are changing during the training. Nevertheless, the following iterative procedure can be adopted to update γ such that the trained NODE remains contractive during training: i) perform a forward propagation through the CH-NODE with the current value of γ and weights and calculate the training loss, ii) update the weights via backpropagation, iii) calculate c_1 and c_2 for the new weights and update γ . In the sequel, we refer to the NODE (12) as CH-NODE.

B. Non-exploding gradients

From the implementation point of view, neural ODEs may have vanishing or exploding gradients during training, which may cause numerical instability. These phenomena are related to the convergence to zero or the divergence, respectively, of the Backward Sensitivity Matrices (BSMs) arising in gradient computations through backpropagation [21]. The continuous-time BSM for the NODE (12) is defined as

$$\frac{\partial \boldsymbol{\xi}(T)}{\partial \boldsymbol{\xi}(T-t)}, \quad \forall t \in [0, T]. \quad (13)$$

Note that the BSM represents the sensitivity of the output with respect to the intermediate state (hidden continuum) of a NODE. This term is used to update the NODE parameters during gradient descent [21]. Therefore, if the norm $\left\| \frac{\partial \boldsymbol{\xi}(T)}{\partial \boldsymbol{\xi}(T-t)} \right\|$ is too small or too large, the vanishing/exploding

gradients may appear and render the learning process unreliable.

In the following, we show that CH-NODEs (12) have built-in guarantees of non-exploding gradients. The result is stated in the following theorem, whose proof is given in Appendix VI-B.

Theorem 2: The BSM (13) associated with the CH-NODE (12) satisfies

$$\exp(-\rho T) \leq \left\| \frac{\partial \boldsymbol{\xi}(T)}{\partial \boldsymbol{\xi}(T-t)} \right\| \leq 1, \quad (14)$$

where $t \in [0, T]$, $\rho = \frac{\epsilon\beta(\gamma^2 + \bar{\lambda}(\mathbf{J}\mathbf{J}^\top))}{2\gamma}$, $\beta = \frac{1}{2}(c_1 + c_2)$, $\epsilon > 0$, and $\|\cdot\|$ is any sub-multiplicative norm.

Note that in (14) the lower bound converges to zero exponentially, which may cause vanishing gradients. Nevertheless, one can properly select ϵ and T to avoid this problem.

IV. EXPERIMENTS

In this section, first we show how contractivity improves the robustness of NODEs through a 2D binary classification example. Second, we demonstrate the effectiveness of the CH-NODE (12) on the MNIST image classification task and compare the performance with residual networks (ResNets) [22] and Hamiltonian deep neural networks (H-DNNs) [21]. Third, we numerically validate the non-exploding gradients properties of CH-NODEs².

A. Contractivity promotes robustness

To build an intuition on how contractivity promotes robustness, we compared a vanilla NODE and a time-invariant CH-NODE³ on a 2D binary classification task. By using a linear *softmax* classifier as the output layer, we trained both NODEs to achieve a training accuracy of 100% to classify the two sets of points (red and blue) shown in Fig 1. The classification results for the vanilla NODE and the CH-NODE are illustrated in Fig. 1a, and Fig. 1c, respectively, where the colored regions represent the predictions of the trained NODEs. It is clear from Fig. 1a that the blue training points are closer to the classification boundary compared to Fig. 1d. Therefore, a small perturbation of the training set can result in a wrong prediction for the vanilla NODE. However, since the training points are farther from the classification boundary in Fig. 1c, the CH-NODE is expected to be more robust to small perturbations.

This is confirmed by Fig. 1b and Fig. 1d representing the flows of the vanilla NODE and the CH-NODE, respectively, after training. We further selected a small set of points (purple circles) around the training points and propagate them to the corresponding outputs of the NODEs (orange sets) as shown in Fig. 1b and Fig. 1d. One can notice that, with the vanilla NODE, the propagated orange set crosses the classification hyperplane (the black dashed line). As a consequence, a slight perturbation would make the vanilla NODE to generate wrong predictions. On the other hand,

²The technical details and our code are available at <https://github.com/DecodEPFL/Contractive-Hamiltonian-Neural-ODEs>

³Setting $\mathbf{K}(t) = \mathbf{K}$, $\mathbf{b}(t) = \mathbf{b}$, $\mathbf{L}(t) = 0$ as constant matrices in (12)

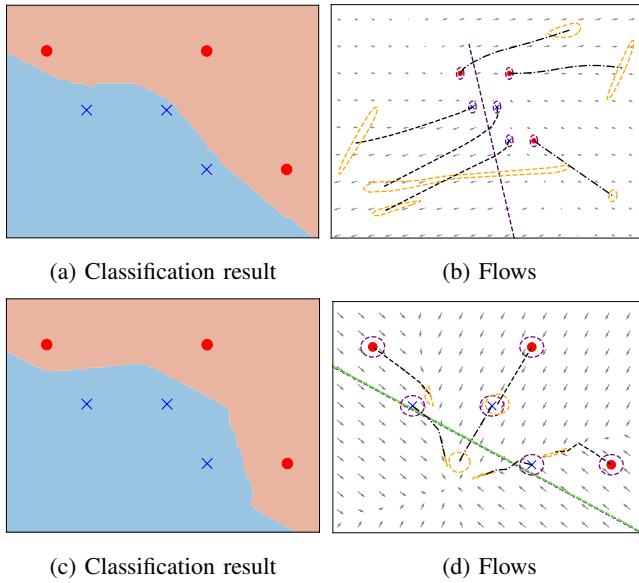


Fig. 1: Comparison between a vanilla NODE (Fig. (1a), and (1b)) and a CH-NODE (Fig. (1c), and (1d)) on a 2D binary classification task. The quiver lines show the flows of NODEs, and the black dashed lines show propagation of training data points in time.

Fig. 1d shows that after the forward propagation through the CH-NODE, the size of purple circles either remains the same, or shrinks and still lies in on a single side of the classification hyperplane (the green dashed line).

B. MNIST Classification

We consider the digit recognition problem using the MNIST [23] dataset, and compare the robustness of the proposed NODEs with other standard neural networks. Following [24], and [21], we employ a network architecture consisting of: i) a convolutional layer (input layer), followed by ii) NODE (continuum of hidden layer), and iii) a *softmax* output layer.

We compare the performance of the CH-NODE with the ResNet and the H-DNN proposed in [21], which has a similar structure to the CH-NODE. For the implementation, we used FE discretization method (4) with a step size of $h = 0.5$ and to have comparable numbers of trainable parameters in all networks, we set $L = 0$ and $\kappa = 4 \times 10^{-4}$ in (8). We obtain the following NN architectures

$$\begin{aligned}
 \text{ResNet: } & \xi_{i+1} = \xi_i + h \tanh(\mathbf{K}_i \xi_i + \mathbf{b}_i) \\
 \text{H-DNN: } & \xi_{i+1} = \xi_i + h \mathbf{J} \mathbf{K}_i^T \tanh(\mathbf{K}_i \xi_i + \mathbf{b}_i) \\
 \text{C-HNN: } & \xi_{i+1} = (\mathbf{I} + \kappa h \mathbf{F}) \xi_i + h \mathbf{F} \mathbf{K}_i^T \tanh(\mathbf{K}_i \xi_i + \mathbf{b}_i) \\
 & \text{for } i = 0, 1, \dots, N-1,
 \end{aligned}$$

where N is the number of layers, $\mathbf{F} = \mathbf{J} - \gamma \mathbf{I}$ and $\mathbf{J} = \begin{bmatrix} \mathbf{0} & \mathbf{I} \\ -\mathbf{I} & \mathbf{0} \end{bmatrix}$ has suitable dimensions.

Since γ depends upon the weights, it is necessary to update γ after each iteration to ensure contractivity during the training. This is achieved as follows: i) perform a forward propagation with the current value of γ and

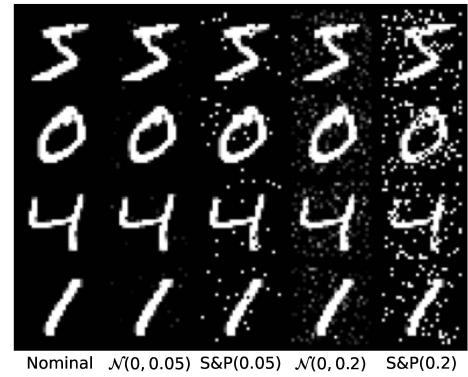


Fig. 2: Corrupted MNIST test samples for the classification

weights and compute the cross-entropy loss, ii) update the weights via backpropagation, iii) compute $c_1 = \kappa$ and $c_2 = \max_{i=1, \dots, N-1} (\lambda(\mathbf{K}_i^T \mathbf{K}_i) + \kappa)$ for the updated weights, and finally, iv) compute and update γ as in (11) using c_1 and c_2 .

The robustness of NNs can be evaluated through the lens of their performance on perturbed images. Thus, we corrupted the test dataset with two types of noises of various magnitudes to compare the robustness. Specifically, we chose zero-mean Gaussian noise $\mathcal{N}(0, \sigma)$, and the salt and pepper noise $s\&p(\sigma)$ with $\sigma = [0.05, 0.2]$ [25]. For the Gaussian noise σ denotes the variance, and for $s\&p$, σ denotes the percentage of corrupted pixels with the impulse noise (white or black pixel). Thus, we have four different datasets: a few samples from each case are shown in Fig. 2.

The trained networks were tested against 10,000 noisy test samples in four experiments. For each experiment, ten noisy test datasets were generated and the corresponding averaged accuracy for each architecture is given in Table I. We can see that, for each case, the test accuracy for ResNet and H-DNNs reduces significantly on the noisy test datasets. On the other hand, C-HNNs show an improvement in the test accuracy for all noisy scenarios. This supports our claim, that indeed, contractivity enhances robustness against small perturbations. Moreover, we can observe a decreasing trend in the train and test accuracy of C-HNNs as the number of layers increases, which is consistent with Remark 2.

C. Numerical validation of non-exploding gradients

We demonstrate the non-exploding gradients property of CH-NODEs on the ‘‘Double circles’’ dataset used in [21]. We discretize the ODE (12) using FE method with a step-size of $h = 6.25 \times 10^{-4}$ to obtain the C-HNN with 16 layers, each with inputs and outputs in \mathbb{R}^2 . We set $L = 0$ and $\kappa = 0.04$ in (12), and choose $\epsilon = 1.0 \times 10^{-9}$. We analyze the norm of BSMs during the training and results are displayed in Fig. 3. It is easy to see that the norm of BSM remains bounded between $0.3214 \leq \|\frac{\partial \xi(T)}{\partial \xi(T-t)}\| \leq 1$. Moreover, we achieved a good performance with the train accuracy of 99.20% and the test accuracy of 99.12%.

N		Nominal		$\mathcal{N}(0, \sigma)$		s&p(σ)	
		Train	Test	$\sigma = 0.05$	$\sigma = 0.2$	$\sigma = 0.05$	$\sigma = 0.2$
2	ResNet	97.89	96.70	15.16	13.91	15.96	14.85
	H-DNN	95.42	95.56	66.07	60.84	66.63	54.07
	C-HNN	98.29	96.12	76.61	67.89	69.90	41.45
4	ResNet	98.37	97.35	49.68	42.94	47.36	34.29
	H-DNN	96.34	96.09	21.2	16.94	22.12	17.64
	C-HNN	93.67	92.01	83.94	71.32	81.40	61.12
6	ResNet	98.06	97.21	57.10	50.69	55.62	43.77
	H-DNN	96.60	96.20	27.09	25.26	26.56	23.10
	C-HNN	91.97	91.90	81.73	76.69	82.86	73.14
8	ResNet	96.86	98.24	29.69	27.73	28.64	24.18
	H-DNN	95.99	94.87	56.26	52.05	52.48	40.49
	C-HNN	89.67	88.81	86.14	85.12	85.27	75.66

TABLE I: Robustness comparison between ResNets, H-DNNs, and C-HNNs under the zero-mean Gaussian and the salt and pepper noise. For each value of N , the best performance in each column appears in **bold**.

V. CONCLUSIONS

We proposed NODEs based on Hamiltonian dynamics that are contractive by design. Our parameterization lifts the need of stability promoting cost/regularizers, hence, improves the computational efficiency. Furthermore, we have shown that, during the training, the BSM is always upper bounded by 1. The robustness of these networks against input noise has been validated using benchmark classification examples.

Further research will be devoted to analyze the robustness of CH-NODEs against different forms of adversarial attacks, such as fast gradient sign method (FSGM).

VI. APPENDIX

A. Proof of Theorem 1

The Hessian of the Hamiltonian function (8) is

$$\frac{\partial^2 H(\boldsymbol{\xi}, t)}{\partial \boldsymbol{\xi}^2} = \mathbf{K}^\top(t) \mathbf{D}(\boldsymbol{\xi}, t) \mathbf{K}(t) + \mathbf{L}^\top(t) \mathbf{L}(t) + \kappa \mathbf{I},$$

where $\mathbf{D}(\boldsymbol{\xi}, t) = \text{diag}(\tanh'(\mathbf{K}(t)\boldsymbol{\xi} + \mathbf{b}(t)))$ is a diagonal matrix. By exploiting the properties of $\tanh'(\cdot)$, we can bound this diagonal matrix as $\mathbf{0} \leq \mathbf{D}(\boldsymbol{\xi}, t) \leq \mathbf{I}$. Therefore, we have

$$0 < c_1 \mathbf{I} \leq \frac{\partial^2 H(\boldsymbol{\xi}, t)}{\partial \boldsymbol{\xi}^2} \leq c_2 \mathbf{I}, \quad (15)$$

where the constants c_1 and c_2 are defined in (9) and (10), respectively.

Denote $\bar{\lambda}_J = \bar{\lambda}(\mathbf{J}\mathbf{J}^\top)$, if γ is selected to satisfy (11), after some manipulations, we have

$$-\frac{\gamma^2}{(\gamma^2 + \lambda_J)^2} + \frac{\alpha^2 + \epsilon}{\gamma^2 + \lambda_J} \leq 0. \quad (16)$$

Let $\nu = \frac{\gamma}{\gamma^2 + \lambda_J} > 0$, and add $(\nu - \frac{\gamma}{\gamma^2 + \lambda_J})^2$ to the LHS of (16) to obtain

$$\left(\nu - \frac{\gamma}{\gamma^2 + \lambda_J}\right)^2 - \frac{\gamma^2}{(\gamma^2 + \lambda_J)^2} + \frac{\alpha^2 + \epsilon}{\gamma^2 + \lambda_J} \leq 0$$

which after some manipulations is

$$\nu^2(\gamma^2 + \lambda_J) - 2\nu\gamma + \alpha^2 + \epsilon \leq 0.$$

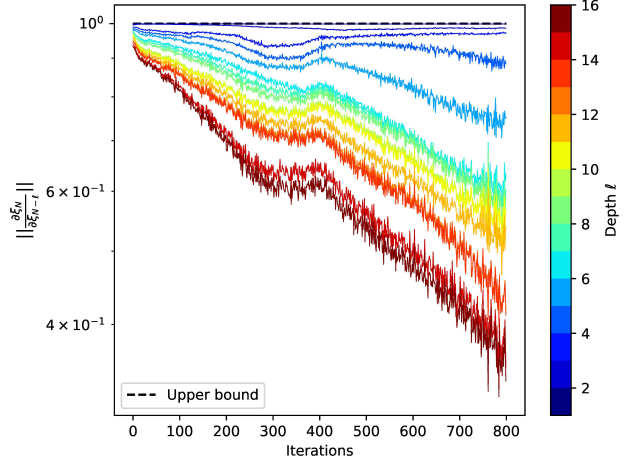


Fig. 3: Evolution of the 2-norm of the BSM during the training of a 16-layer C-HNN exhibiting non-exploding gradients.

Since $\mathbf{J}\mathbf{J}^\top \leq \bar{\lambda}_J \mathbf{I}$, we further have

$$-2\nu\gamma \mathbf{I} + \alpha^2 \mathbf{I} + \epsilon \mathbf{I} + \nu^2 \mathbf{J}\mathbf{J}^\top + \gamma^2 \nu^2 \mathbf{I} \leq 0. \quad (17)$$

By exploiting the skew-symmetric property $\mathbf{J} + \mathbf{J}^\top = \mathbf{0}$, it is straightforward to show that (17) is equivalent to

$$\nu(\mathbf{J} - \gamma \mathbf{I}) + \nu(\mathbf{J} - \gamma \mathbf{I})^\top + \alpha^2 \mathbf{I} + \epsilon \mathbf{I} + \nu^2(\mathbf{J} - \gamma \mathbf{I})(\mathbf{J} - \gamma \mathbf{I})^\top \leq 0.$$

By defining $\mathbf{F} = \mathbf{J} - \gamma \mathbf{I}$ and $\mathbf{P} = \nu \mathbf{I}$, we can write the above inequality as

$$\mathbf{P}\mathbf{F} + \mathbf{F}^\top \mathbf{P} + \alpha^2 \mathbf{I} + \epsilon \mathbf{I} + \mathbf{P}\mathbf{F}\mathbf{F}^\top \mathbf{P} \leq 0, \quad (18)$$

which is equivalent to the following by using the Schur complement lemma

$$\begin{bmatrix} \mathbf{P}\mathbf{F} + \mathbf{F}^\top \mathbf{P} + \alpha^2 \mathbf{I} + \epsilon \mathbf{I} & \mathbf{P}\mathbf{F} \\ \star & -\mathbf{I} \end{bmatrix} \leq 0. \quad (19)$$

Then in view of Proposition 3 in [26] and (15), we know that the Hamiltonian system (12) is contractive. The proof is completed.

B. Proof of Theorem 2

Define $\Phi(T, T-t) = \frac{\partial \boldsymbol{\xi}(T)}{\partial \boldsymbol{\xi}(T-t)}$, following the derivations in [21, Appendix III], we have

$$\dot{\Phi}(T, T-t) = \mathbf{A}(T-t)\Phi(T, T-t), \quad (20)$$

where $t \in [0, T]$ and

$$\mathbf{A}(T-t) = (\mathbf{J} - \gamma \mathbf{I}) \frac{\partial^2 H(\boldsymbol{\xi}(T-t), T-t, \theta)}{\partial \boldsymbol{\xi}^2(T-t)}. \quad (21)$$

For the sake of brevity, we denote $\Phi := \Phi(T, T-t)$, and further define

$$\begin{aligned} \mathbf{X}(T-t) &:= \frac{\partial^2 H(\boldsymbol{\xi}(T-t), T-t, \theta)}{\partial \boldsymbol{\xi}^2(T-t)} - \beta \mathbf{I} \\ \boldsymbol{\zeta}(T-t) &= \mathbf{X}(T-t)\Phi, \end{aligned}$$

where $\beta = \frac{1}{2}(c_1 + c_2)$. Then, (20) can be rewritten as

$$\dot{\Phi} = \beta(\mathbf{J} - \gamma\mathbf{I})\Phi + (\mathbf{J} - \gamma\mathbf{I})\zeta(T - t). \quad (22)$$

For CH-NODE, the matrix inequality (19) holds with $\mathbf{P} = \nu\mathbf{I}$, where $\nu = \frac{\gamma}{\gamma^2 + \lambda J}$. It is easy to see that (19) implies,

$$\begin{bmatrix} \beta\Phi^\top \\ \zeta^\top \end{bmatrix}^\top \begin{bmatrix} \nu\mathbf{F} + \nu\mathbf{F}^\top + \alpha^2\mathbf{I} + \epsilon\mathbf{I} & \nu\mathbf{F} \\ \star & -\mathbf{I} \end{bmatrix} \begin{bmatrix} \beta\Phi \\ \zeta \end{bmatrix} \leq 0, \quad (23)$$

where we denoted $\zeta := \zeta(T - t)$ for simplicity. Using Schur complement lemma and after some calculation, we have

$$2\nu\beta\Phi^\top(\beta\mathbf{F}\Phi + \mathbf{F}\zeta) + \alpha^2\beta^2\Phi^\top\Phi - \zeta^\top\zeta \leq -\epsilon\beta^2\Phi^\top\Phi. \quad (24)$$

Define the function $\mathbf{V}(T, T - t) = \Phi^\top V(0)\Phi$, where $V(0) = \nu\beta\mathbf{I} > 0$, and denote $\mathbf{V} := \mathbf{V}(T, T - t)$ as a shorthand notation. Then, we have the following differential equation along the trajectories of (20) or (22)

$$\dot{\mathbf{V}} = \mathbf{A}(T - t)\mathbf{V} + \mathbf{V}\mathbf{A}^\top(T - t). \quad (25)$$

Thus, using (25), we can write (24) as

$$\dot{\mathbf{V}} + \mu^2\Phi^\top\Phi - \zeta^\top\zeta \leq -\delta\Phi^\top\Phi, \quad (26)$$

where $\mu^2 = \alpha^2\beta^2$, and $\delta = \epsilon\beta^2$. Moreover, from (15), the following holds

$$-\mu\mathbf{I} \leq \mathbf{X}(T - t) \leq \mu\mathbf{I}, \quad \mu = \frac{1}{2}(c_2 - c_1),$$

which implies

$$\mu^2\Phi^\top\Phi - \zeta^\top\zeta \geq 0. \quad (27)$$

By substituting (27) into (26), we get $\dot{\mathbf{V}} \leq \delta\Phi^\top\Phi$

$$\dot{\mathbf{V}} \leq \delta\Phi^\top\Phi = -2\left(\frac{\delta}{2\nu\beta}\right)\nu\beta\Phi^\top\Phi = -2\left(\frac{\epsilon\beta}{2\nu}\right)\mathbf{V} = -2\rho\mathbf{V},$$

where $\rho = \frac{\epsilon\beta(\gamma^2 + \lambda(JJ^\top))}{2\gamma}$. Therefore, $\text{tr}(\dot{\mathbf{V}}) \leq -2\rho\text{tr}(\mathbf{V})$, which means \mathbf{V} is decreasing exponentially in time. The norm of BSM matrix will also converge exponentially according to the following inequality, [15]

$$\|\Phi(T, T - t)\| \leq \|\Phi(T, T)\| \times \exp(-\rho(T - t)).$$

By substituting the value of $t = 0$, and $t = T$, we can obtain lower and upper bound, respectively. Since $\Phi(T, T) = \mathbf{I}$, the sub-multiplicative norm of the gradients is upper bounded by 1.

REFERENCES

- [1] H. Xu, Y. Ma, H.-C. Liu, D. Deb, H. Liu, J.-L. Tang, and A. K. Jain, "Adversarial attacks and defenses in images, graphs and text: A review," *International Journal of Automation and Computing*, vol. 17, no. 2, pp. 151–178, 2020.
- [2] C. Szegedy, W. Zaremba, I. Sutskever, J. Bruna, D. Erhan, I. Goodfellow, and R. Fergus, "Intriguing properties of neural networks," *arXiv preprint arXiv:1312.6199*, 2013.
- [3] D. J. Miller, Z. Xiang, and G. Kesidis, "Adversarial learning targeting deep neural network classification: A comprehensive review of defenses against attacks this article provides a contemporary survey of defenses against adversarial learning (al), focused particularly on defenses against attacks on deep neural network classifiers," *Proceedings of the IEEE*, 2020.

- [4] I. J. Goodfellow, J. Shlens, and C. Szegedy, "Explaining and harnessing adversarial examples," *arXiv preprint arXiv:1412.6572*, 2014.
- [5] M. Fazlyab, A. Robey, H. Hassani, M. Morari, and G. Pappas, "Efficient and accurate estimation of lipschitz constants for deep neural networks," in *Advances in Neural Information Processing Systems*, Conference Proceedings, pp. 11 423–11 434.
- [6] B. Aquino, A. Rahnama, P. Seiler, L. Lin, and V. Gupta, "Robustness against adversarial attacks in neural networks using incremental dissipativity," *IEEE Control Systems Letters*, pp. 1–1, 2022.
- [7] E. Haber and L. Ruthotto, "Stable architectures for deep neural networks," *Inverse Problems*, vol. 34, no. 1, p. 014004, 2017.
- [8] R. T. Chen, Y. Rubanova, J. Bettencourt, and D. K. Duvenaud, "Neural ordinary differential equations," in *Advances in neural information processing systems*, vol. 31, 2018, pp. 6571–6583.
- [9] Y. Rubanova, R. T. Chen, and D. K. Duvenaud, "Latent ordinary differential equations for irregularly-sampled time series," *Advances in neural information processing systems*, vol. 32, 2019.
- [10] S. Greydanus, M. Dzamba, and J. Yosinski, "Hamiltonian neural networks," *Advances in Neural Information Processing Systems*, vol. 32, 2019.
- [11] H. YAN, J. DU, V. TAN, and J. FENG, "On robustness of neural ordinary differential equations," in *International Conference on Learning Representations*, 2020.
- [12] Q. Kang, Y. Song, Q. Ding, and W. P. Tay, "Stable neural ode with lyapunov-stable equilibrium points for defending against adversarial attacks," *Advances in Neural Information Processing Systems*, vol. 34, 2021.
- [13] Ivan, Aaron, and Y. Yue, "LyaNet: A Lyapunov framework for training neural ODEs," *arXiv pre-print server*, 2022.
- [14] W. Lohmiller and J.-J. E. Slotine, "On contraction analysis for nonlinear systems," *Automatica*, vol. 34, no. 6, pp. 683–696, 1998.
- [15] H. Tsukamoto, S.-J. Chung, and J.-J. E. Slotine, "Contraction theory for nonlinear stability analysis and learning-based control: A tutorial overview," *Annual Reviews in Control*, vol. 52, pp. 135–169, 2021.
- [16] S. Jafarpour, A. Davydov, A. Proskurnikov, and F. Bullo, "Robust implicit networks via non-euclidean contractions," *Advances in Neural Information Processing Systems*, vol. 34, 2021.
- [17] M. Revay and I. Manchester, "Contracting implicit recurrent neural networks: Stable models with improved trainability," in *Learning for Dynamics and Control*. PMLR, 2020, pp. 393–403.
- [18] V. Duindam, A. Macchelli, S. Stramigioli, and H. Bruyninckx, *Modeling and control of complex physical systems: the port-Hamiltonian approach*. Springer Science & Business Media, 2009.
- [19] D. Tsipras, S. Santurkar, L. Engstrom, A. Turner, and A. Madry, "Robustness may be at odds with accuracy," in *International Conference on Learning Representations*, 2019.
- [20] A. van der Schaft, *L2-gain and passivity techniques in nonlinear control*. Springer, 2017, vol. 2.
- [21] C. L. Galimberti, L. Furiieri, L. Xu, and G. Ferrari-Trecate, "Hamiltonian deep neural networks guaranteeing non-vanishing gradients by design," *arXiv preprint arXiv:2105.13205*, 2021.
- [22] K. He, X. Zhang, S. Ren, and J. Sun, "Deep residual learning for image recognition," in *Proceedings of the IEEE conference on computer vision and pattern recognition*, 2016, pp. 770–778.
- [23] L. Deng, "The MNIST database of handwritten digit images for machine learning research," *IEEE signal processing magazine*, vol. 29, no. 6, pp. 141–142, 2012.
- [24] E. Haber and L. Ruthotto, "Stable architectures for deep neural networks," *Inverse problems*, vol. 34, no. 1, p. 014004, 2017.
- [25] L. Schott, J. Rauber, M. Bethge, and W. Brendel, "Towards the first adversarially robust neural network model on MNIST," in *International Conference on Learning Representations*, 2019.
- [26] N. Barabanov, R. Ortega, and A. Pyrkin, "On contraction of time-varying port-Hamiltonian systems," *Systems & Control Letters*, vol. 133, p. 104545, 2019.